

Particle acceleration in relativistic magnetic reconnection with strong inverse-Compton cooling in pair plasmas

Gregory R. Werner,^{1*} Alexander A. Philippov,^{2†} Dmitri A. Uzdensky,¹

¹Center for Integrated Plasma Studies, Physics Department, 390 UCB, University of Colorado, Boulder, CO 80309, USA

²Astronomy Department, University of California, Berkeley, 601 Campbell Hall, Berkeley, CA 94720, USA

25 November 2021

ABSTRACT

Particle-in-cell (PIC) simulations have shown that relativistic collisionless magnetic reconnection drives nonthermal particle acceleration (NTPA), potentially explaining high-energy (X-ray/ γ -ray) synchrotron and/or inverse Compton (IC) radiation observed from various astrophysical sources. The radiation back-reaction force on radiating particles has been neglected in most of these simulations, even though radiative cooling considerably alters particle dynamics in many astrophysical environments where reconnection may be important. We present a radiative PIC study examining the effects of external IC cooling on the basic dynamics, NTPA, and radiative signatures of relativistic reconnection in pair plasmas. We find that, while the reconnection rate and overall dynamics are basically unchanged, IC cooling significantly influences NTPA: the particle spectra still show a hard power law (index ≥ -2) as in nonradiative reconnection, but transition to a steeper power law that extends to a cooling-dependent cutoff. The steep power-law index fluctuates in time between roughly -3 and -5 . The time-integrated photon spectra display corresponding power laws with indices ≈ -0.5 and ≈ -1.1 , similar to those observed in hard X-ray spectra of accreting black holes.

Key words: acceleration of particles – accretion, accretion discs – magnetic reconnection – radiation mechanisms: general – X-rays: binaries – galaxies: jets

1 INTRODUCTION

Spectacular high-energy flares in various astrophysical sources are often believed to be powered by magnetic reconnection – a fundamental plasma process of rapid magnetic field reorganization accompanied by a violent release of magnetic energy and its conversion to plasma energy (e.g., Zweibel & Yamada 2009). In many systems, reconnection occurs in the relativistic regime, where magnetic energy density exceeds the total (including rest-mass) energy density of the plasma (Lyutikov & Uzdensky 2003; Lyubarsky 2005), generating relativistic flows, heating the plasma to relativistic temperatures, and driving ultrarelativistic nonthermal particle acceleration (NTPA) (Hoshino & Lyubarsky 2012; Kagan et al. 2015). Due to its broad astrophysical relevance, relativistic reconnection has been studied extensively, including via particle-in-cell (PIC) simulations. So far, most of these studies have ignored any radiative aspects of reconnection. However, in many high-energy astrophysical environments, the radiation reaction (which we call *radiation*

for short) force on the particles can strongly affect the dynamics, energetics, NTPA, and radiative signatures of reconnection (Uzdensky 2016). The two main radiative processes in astrophysical reconnection are synchrotron emission (e.g., in pulsar magnetospheres, Lyubarsky 1996; Uzdensky & Spitkovsky 2014; Cerutti et al. 2016; Philippov & Spitkovsky 2018 and pulsar wind nebulae, Uzdensky et al. 2011; Cerutti et al. 2013) and inverse-Compton (IC) scattering [e.g., in black-hole (BH) accretion disc coronae (ADCe) in X-ray Binaries (XRBs) and active galactic nuclei (AGN), Goodman & Uzdensky 2008; Beloborodov 2017, and also in AGN (e.g., blazar) jets]. While several pioneering PIC studies have investigated reconnection with synchrotron cooling (Jaroschek & Hoshino 2009; Cerutti et al. 2013, 2016; Kagan et al. 2016; Yuan et al. 2016), IC cooling effects on reconnection have not yet been explored [since submission of this manuscript, Nalewajko et al. (2018) have also studied IC cooling].

Here we present the first systematic numerical study of relativistic collisionless reconnection with optically-thin external IC cooling. Using two PIC codes that incorporate the IC radiation force, TRISTAN-MP and ZELTRON, we show how reconnection-driven NTPA and resulting radiation sig-

* E-mail: greg.werner@colorado.edu

† Einstein Fellow

Table 1. Simulation parameters constant over this study.

| | |
|-------------------------------|--|
| nominal gyroradius | $\rho_0 = m_e c^2 / e B_0$ |
| initial guide magnetic field | $B_{gz} = B_0 / 4$ |
| “hot” magnetization | $\sigma_h \equiv B_0^2 / (16\pi n_b T_b) = 100$ |
| “cold” magnetization | $\sigma \equiv B_0^2 / (4\pi n_b m_e c^2) = 10^4$ |
| peak Harris layer density | $n_{d0} = \eta n_b = 5 n_b$ |
| Harris layer drift velocity | $\pm \beta_d c \hat{z} = \pm 0.3 c \hat{z}$ |
| Harris layer (comoving) temp. | $T_d / m_e c^2 = \gamma_d \sigma / 2\eta = 1050$ |
| Harris layer half-thickness | $\delta = \sigma \rho_0 / (\eta \beta_d) = 0.67 \sigma \rho_0$ |
| cell size | $\Delta x = \Delta y = \sigma \rho_0 / 24$ |
| total macroparticles per cell | 10 |
| time step | $\Delta t = 0.45 \Delta x / c$ |
| simulation time | $T = 5 L_x / c$ |

natures change due to the IC drag as accelerated particles scatter off an imposed soft photon bath; we systematically vary the IC cooling via the imposed soft photon density, which represents, e.g., in BH ADCe in the High-Soft (HS) state of XRBs, the thermal X-rays from the accretion disc. We limit this first study to e^+e^- pair plasmas, leaving the more XRB-relevant electron-ion case for the future. Since previous studies have shown that 2D and 3D PIC simulations of non-radiative pair-plasma reconnection yield very similar NTPA (Werner & Uzdensky 2017), we use 2D simulations to enable exploration of larger systems.

2 NUMERICAL SIMULATION SETUP

We use a standard double-periodic box with two relativistic Harris pair-plasma current sheets (Kirk & Skjæraasen 2003), plus a uniform background pair plasma of total (e^- and e^+) density n_b and temperature $T_b = 25 m_e c^2$, reflecting the ambient upstream conditions. The box dimensions are $L_x \times L_y$ ($L_y = 2L_x$), with x parallel to the reconnecting magnetic field B_0 and y perpendicular to the current sheets; z (not simulated) is the initial sheet current direction. All key parameters are described fully in Werner & Uzdensky (2017) and briefly in Table 1 in terms of B_0 , n_b , and T_b . Reconnection is gently kick-started with a small (10^{-2}) magnetic field perturbation as in Werner & Uzdensky (2017). We present results for $L_x / \sigma \rho_0 = 320$, well in the large-system regime (Werner et al. 2016) where the high-energy cutoff of the particle spectrum no longer grows linearly with L_x .

Our codes TRISTAN-MP (Spitkovsky 2005) and ZELTRON (Cerutti et al. 2013) use standard PIC algorithms, explicitly evolving Maxwell’s equations on a grid with currents self-consistently calculated from particles moving via the Lorentz force. In addition, they include the back-reaction force on particles emitting IC radiation (Tamburini et al. 2010).

The IC drag force, felt by an electron or positron with velocity $c\beta$ and energy $\gamma m_e c^2$ as it upscatters photons from an isotropic radiation bath of energy density U_{ph} , is $\mathbf{f}_{\text{IC}} = -(4/3)\sigma_T U_{\text{ph}} \gamma^2 \beta$, where $\sigma_T = 8\pi e^4 / (3m_e^2 c^4)$. Balancing \mathbf{f}_{IC} against the accelerating force of the reconnection electric field $E = \beta_{\text{rec}} B_0$, and taking $\beta_{\text{rec}} \sim 0.1$ for relativistic reconnection, yields the radiation limit:

$$\gamma \lesssim \gamma_{\text{rad}} \equiv \sqrt{3(0.1)eB_0 / (4\sigma_T U_{\text{ph}})}. \quad (1)$$

IC cooling, controlled by U_{ph} , is conveniently quantified by γ_{rad} , since $|\mathbf{f}_{\text{IC}}| \approx 0.1eB_0 (\gamma/\gamma_{\text{rad}})^2$ for $|\beta| \approx 1$.

We ran seven simulations differing only in U_{ph} : $\gamma_{\text{rad}}/\sigma$

$= 1, 2, 4, 6, 8, 16$, and ∞ (no radiation) – a wide-ranging exploration, since $|\mathbf{f}_{\text{IC}}| \sim \gamma_{\text{rad}}^{-2}$. Stronger radiation, $\gamma_{\text{rad}} \ll \sigma$, would (for $\sigma_h = 100$) cool the upstream plasma before it reaches the current layer, causing the upstream parameters to vary in time and changing the nature of the problem.

3 RESULTS

Reconnection Dynamics and Energetics. Reconnection begins as the tearing instability breaks up the current layer into chains of magnetic islands (plasmoids) separated by magnetic X-points. Over time, plasmoids merge into larger ones, while secondary current sheets between them succumb to secondary tearing, yielding a hierarchical structure of X-points and plasmoids (Bhattacharjee et al. 2009; Uzdensky et al. 2010). This familiar picture remains largely unchanged by IC cooling; reconnection continues to perform its most basic function, converting magnetic energy to particle kinetic energy, almost regardless of radiation; radiative cooling merely converts some of that particle energy to radiation.

Although IC cooling strongly affects particles that gain high energies during reconnection, it has little effect on the overall reconnection dynamics and energy conversion, which are evidently controlled by the lower-energy particles that, for $\gamma_{\text{rad}} \gtrsim \sigma$, experience negligible cooling (cf. §2). Notably, as shown in Fig. 1(a), magnetic energy release proceeds nearly independently of IC cooling and we see no discernible effect of radiation on the reconnection rate, $\beta_{\text{rec}} \sim 0.15$. There is, however, a modest effect of radiation on magnetic dissipation: reconnection with strong radiation converts slightly more transverse magnetic energy to guide-field energy $B_z^2/8\pi$. This is because increased cooling reduces plasma pressure in plasmoids, leading to a stronger compression of the guide magnetic field in them.

Although reconnection converts magnetic to particle energy at essentially the same rate, strong radiative cooling ($\gamma_{\text{rad}} \lesssim 4\sigma$) causes this energy to be promptly radiated away, maintaining the total kinetic energy U_{plasma} at a nearly constant radiation-limited level [Fig. 1(b) shows the evolution of magnetic, plasma, and radiated energies for $\gamma_{\text{rad}} = 2\sigma$]. Therefore, in the strong cooling regime the IC luminosity reaches a universal value $dU_{\text{rad}}/dt \sim 0.1U_{B,xy}/(L_x/c)$.

Fig. 1(c) shows how radiation affects the energy partition between particles and radiation (after about $5L_x/c$, when reconnection is long over). With strong cooling, particles radiate away their energy even as they are accelerated by reconnection. Weaker cooling allows particles to reach higher energies before radiation balances the acceleration due to reconnection. In the limit of very weak cooling, particles are accelerated almost as without cooling, slowly radiating away energy long after exiting the reconnection region.

Particle Acceleration. Recent PIC simulations have clearly shown NTPA driven by relativistic reconnection. Reconnection accelerates a large fraction of particles to high energies $\gamma \gtrsim \sigma$, yielding nonthermal high-energy spectra characterized by a power-law index (slope) p and a high-energy cutoff γ_c . IC drag, which scales as γ^2 , can, however, suppress NTPA at highest energies.

With radiation, high-energy particle spectra $f(\gamma)$ vary more in time and display more complicated forms than the familiar single power law with a high-energy cutoff. To mea-

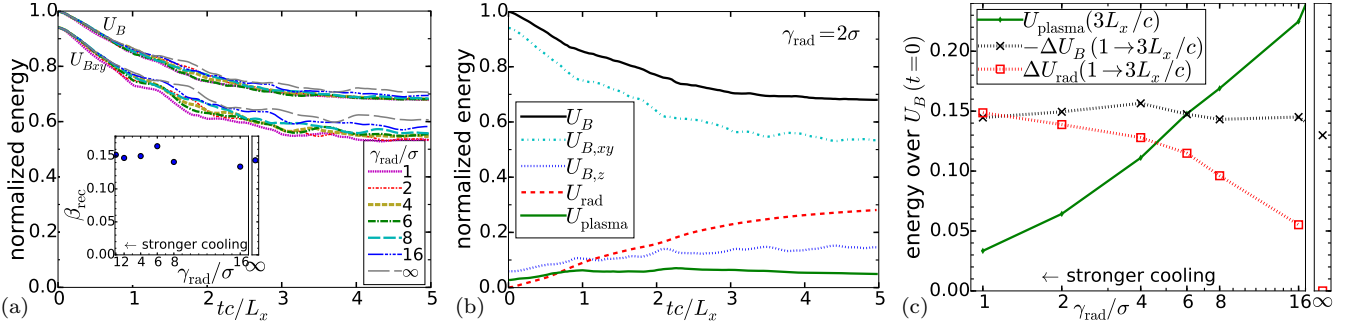


Figure 1. (a) The total and transverse magnetic energy $U_B(t)$ and $U_{B,xy}(t)$ versus time are nearly independent of radiative cooling strength (given by γ_{rad}), and, inset, the normalized reconnection rate is also independent of γ_{rad} . (b) For a strongly-cooled simulation, $\gamma_{\text{rad}} = 2\sigma$, the magnetic energy $U_B(t)$ is similar to weakly-cooled cases, as is the sum of particle U_{plasma} and radiated U_{rad} energies; being strongly-cooled, however, $U_{\text{plasma}}(t)$ quickly saturates, after which any particle energy gains are promptly radiated away. (c) The magnetic energy dissipated between 1 and $3L_x/c$ is independent of cooling strength; for weak cooling, it increases the plasma energy, while for strong cooling it is no sooner given to particles than it is radiated away. All energies are normalized to $U_B(t=0)$.

sure spectral slopes and cutoffs, we calculated the local slope $p(\gamma) = -\ln f/\ln \gamma$ and searched for the longest stretch over which $p(\gamma)$ varied within ± 10 per cent; the next-longest power-law stretch was also identified. We counted only power laws stretching over a factor ≥ 2 in γ , and identified the power-law index p as the median $p(\gamma)$. The high-energy cutoff γ_c was defined by $f(\gamma_c) = e^{-1}A\gamma_c^{-p}$, with $A\gamma^{-p}$ being the best fit for $f(\gamma)$ over the power-law stretch.

Figure 2 shows $f(\gamma)$ at times $tc/L_x = 0, 1.1, 2.2$, and 4.4 for (a) no cooling, (b) moderate cooling, and (c) strong cooling, with power-law fits $f(\gamma) \sim \gamma^{-p}$. Figure 3(a–b) then shows, for all cooling strengths, the complete time-evolution of the fitted power-law indices p and cutoffs γ_c . In the non-radiative case ($\gamma_{\text{rad}} = \infty$) a hard power law quickly develops and remains roughly constant in time (aside from overall amplitude) with index $p_h \approx 1.9$. This agrees with previous studies (e.g., Sironi & Spitkovsky 2014; Guo et al. 2014; Werner et al. 2016) after accounting for the steepening effect of guide field (Werner & Uzdensky 2017) – e.g., we find $p_h \approx 1.6$ for $B_{gz} = 0.05B_0$. The high-energy cutoff rises rapidly to $\gamma_c \simeq 4\sigma$ (as in Werner et al. 2016) and then slowly to $\simeq 10\sigma$ (cf. Petropoulou & Sironi 2018) before reconnection ends around $t \simeq 3L_x/c$. With weak cooling ($\gamma_{\text{rad}} = 16\sigma$) a similar hard power law forms up to (but not beyond) $\gamma_c \simeq 4\sigma$, steepening slightly with time while the cutoff γ_c decreases (as higher-energy particles cool faster). For moderate cooling ($\gamma_{\text{rad}} = 6, 8\sigma$), a hard power law forms at early times with the uncooled $p_h \approx 1.9$, extending initially to $\gamma_c \simeq 4\sigma$. Over time, however, cooling steepens the high-energy part of the power law, yielding a broken power law: the same hard slope $p_h \approx 1.9$ at lower energies, and at higher energies a steeper power law with a highly-variable index [$p_s \approx 4.6$ is shown at $t = 2.2L_x/c$ in Fig. 2(b), but Fig. 3(a) shows that $3 \lesssim p_s \lesssim 5$ at other times]. Over time, cooling shifts the break γ_{br} between power laws toward lower energies until the hard power law disappears. For strong cooling ($\gamma_{\text{rad}} = 1, 2, 4\sigma$), the hard power law appears tenuously at the beginning of active reconnection, but is quickly replaced by the soft/steep power law ($p_s \gtrsim 3$) that dominates the remaining time; as particles no longer being accelerated continue to cool, a low-energy “pile-up” forms, e.g., at $\gamma \simeq 0.04\sigma$ for $t = 4.4L_x/c$ in Fig. 2(c). Although stronger cooling (lower γ_{rad}) reduces the high-energy cutoff to $\gamma_c \sim \gamma_{\text{rad}}$ during active reconnection,

the steep power law index p_s varies over time within roughly the same range (3–5) for all cases $\gamma_{\text{rad}} \lesssim 8\sigma$. Similarly, when visible, $p_h \approx 1.9$ is independent of cooling strength.

In Fig. 3(c) we summarize this picture for the time of active reconnection, roughly $1-3L_x/c$. Independent of γ_{rad} , the hard power-law index is $p_h \approx 1.9$, and the soft power-law index falls in the range $3 < p_s < 5$. While steady-state models for radiatively cooled broken power laws predict an increase of p by 1, reconnection-driven NTPA is non-steady, with bursts of efficient acceleration at X-points followed by cooling. Thus, the soft/steep power law varies in time, reaching a minimum slope of $p_{s,\text{min}} \approx 3 \approx p_h + 1$ occasionally and becoming much steeper than $p_h + 1$ during uninterrupted cooling episodes. Figure 3(c) also shows that the cutoff of the soft/steep power law (when it exists, i.e., for $\gamma_{\text{rad}} \leq 6\sigma$) scales as γ_{rad} . The cutoff of the hard power law (i.e., γ_{br}) decreases with stronger cooling, and the hard power law becomes almost indiscernible for $\gamma_{\text{rad}} \lesssim 4\sigma$.

Radiation. Figure 4 presents IC radiation spectra $F(\epsilon)$ integrated over the simulation time, i.e., over an entire reconnection flare. The power-law index of IC radiation emitted by particles with steady-state power-law index p should be $\alpha_{\text{IC}} = (p-1)/2$, consistent with our measurements $p_h \approx 1.9$ and $\alpha_{\text{IC}} \approx 0.5$ for weak cooling, $\gamma_{\text{rad}} = 16\sigma$. For strong cooling ($\gamma_{\text{rad}} = 2\sigma$), the instantaneous particle and hence photon spectra vary greatly with time. However, periods with harder spectra, $p_s(t) \approx p_{s,\text{min}} \approx 3$, should dominate the overall high-energy emission, i.e., $\alpha_{\text{IC}} \approx (p_{s,\text{min}} - 1)/2 \approx 1$, in agreement with our measured value $\alpha_{\text{IC}} \approx 1.1$.

Code Comparison. TRISTAN-MP and ZELTRON implement essentially the same algorithms, including the IC radiation reaction (§2), but have minor differences, e.g., in charge-conserving current deposition [Umeda et al. (2003) versus Esirkepov (2001)]. Despite wide use in astrophysics, the two codes have not yet been systematically compared; fortunately, we find that they produce essentially identical results for radiative reconnection. Although noisy, the magnetic energy evolution matches closely over long time scales. Crucial to our study of NTPA, the particle spectra are remarkably similar [Fig. 5(a)], agreeing very closely on spectral indices p [Fig. 5(b)] and cutoffs γ_c (not shown) for $\gamma_{\text{rad}} = \infty$. For the strongly-radiative case $\gamma_{\text{rad}} = 2\sigma$, stochastic time

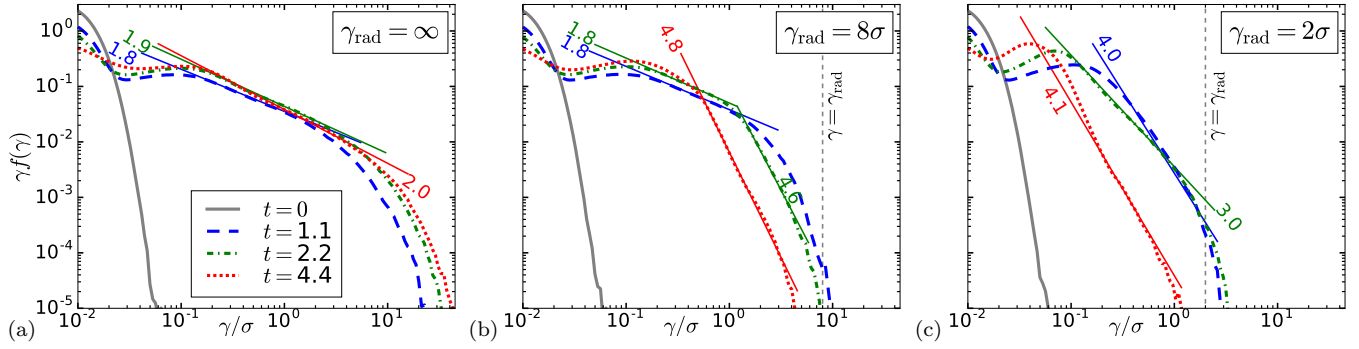


Figure 2. For (a) no cooling, (b) moderate, and (c) strong cooling ($\gamma_{\text{rad}}/\sigma = \infty, 8, 2$), the compensated energy spectra $\gamma f(\gamma)$ are shown at 4 times ($0, 1.1, 2.2, 4.4L_x/c$), with fits $f(\gamma) \sim \gamma^{-p}$ marked with the index p . For $\gamma_{\text{rad}} = 8\sigma$, two power laws are visible at $t = 2.2L_x/c$.

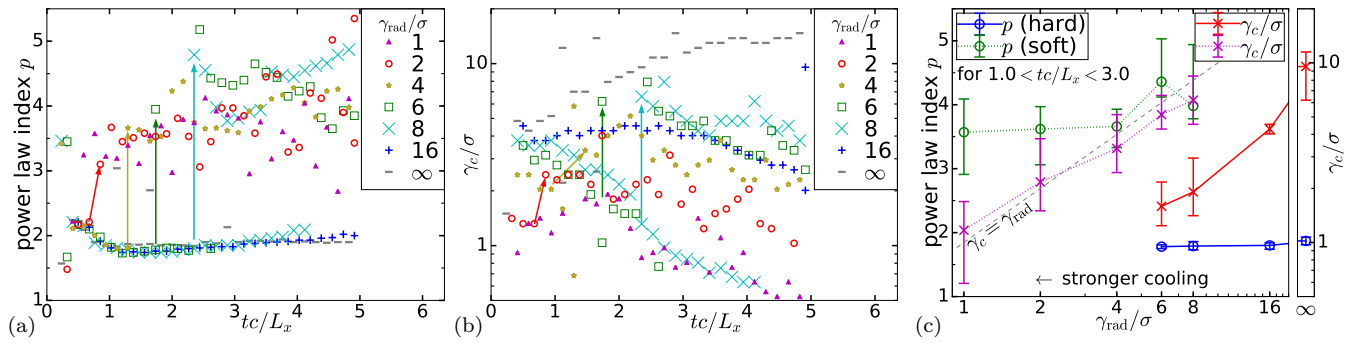


Figure 3. Power-law (a) indices and (b) high-energy cutoffs [where $f(\gamma_c)$ is a factor ϵ below the power-law fit] versus time, for several cooling strengths; if hard and soft power laws appear in the same spectrum, we show p and γ_c for both, connected by an arrow the first time it occurs. (c) The median power-law indices (over hard, $p \leq 2.6$, and soft, $p > 2.6$, power laws) and corresponding cutoffs for spectra during $1 < tc/L_x < 3$, with error bars containing the middle 80 per cent of measurements in this time interval.

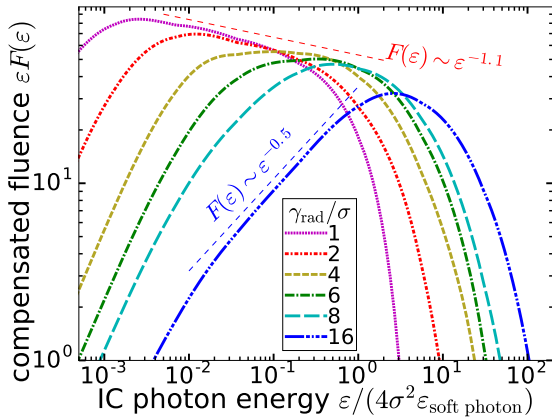


Figure 4. Time-integrated photon spectra (compensated by ϵ) for different cooling strengths. (Note: an electron with γ upscatters an IC photon to maximum energy $4\gamma^2\epsilon_{\text{soft photon}}$, so a $\gamma = \sigma$ electron emits photons of maximum normalized energy 1.)

variation prevents precise comparison at any given time, but both codes yield variation within the same range.

4 CONCLUSIONS

We presented the first systematic numerical study of the effects of the IC radiation reaction (‘radiation’) on magnetic reconnection using first-principles PIC simulation. We

found that, even with strong cooling, basic reconnection dynamics, such as the reconnection rate and magnetic energy dissipation, are unchanged. However, IC cooling strongly affects NTPA and the particle energy spectrum. As a result of radiation, the high-energy spectrum has, in principle, two power laws: for $\gamma < \gamma_{\text{br}}$, a hard slope as in nonradiative simulations ($p_h \simeq 1.8\text{--}2$ for $\sigma_h = 100$ and $B_{gz} = B_0/4$, independent of γ_{rad}), and for $\gamma > \gamma_{\text{br}}$ a steeper slope $p_s \gtrsim 3$. Over time, γ_{br} decreases. For weak radiation ($\gamma_{\text{rad}} \gg 4\sigma$; e.g., $\gamma_{\text{rad}} = 16\sigma$ for the system size studied here), $\gamma_{\text{br}} > 4\sigma$ and only the hard power law appears, with high-energy cutoff $\gamma_c \simeq 4\sigma$. Importantly, even weak radiation prevents the slow growth of γ_c beyond $\simeq 4\sigma$ that occurs without cooling. As radiation is increased and γ_{br} falls below 4σ , both power laws appear simultaneously for a time, with $\gamma_c \simeq \gamma_{\text{rad}}$. For strong radiation ($\gamma_{\text{rad}} \lesssim 4\sigma$), the hard power law is barely detectable. Reflecting the bursty nature of plasmoid-dominated reconnection, the steep power-law index p_s fluctuates strongly, roughly within 3–5, but the hard power-law (p_h), built up over time, is much steadier. Thus, $p_s \gtrsim p_h + 1$, with equality expected for radiative steepening of a continuously injected power law p_h subject to IC cooling, and inequality corresponding to further cooling between acceleration episodes. The IC spectra accordingly have two power laws with slopes of roughly $\alpha_{\text{IC}} \approx (p_h - 1)/2$ and $\alpha_{\text{IC}} \approx (p_{s,\text{min}} - 1)/2 \sim p_h/2$. Lowering the guide field (e.g., to $B_{gz} = 0.05B_0$) yields very similar results but slightly hardens all spectra, as expected (Werner & Uzdensky 2017). While IC and synchrotron radiation

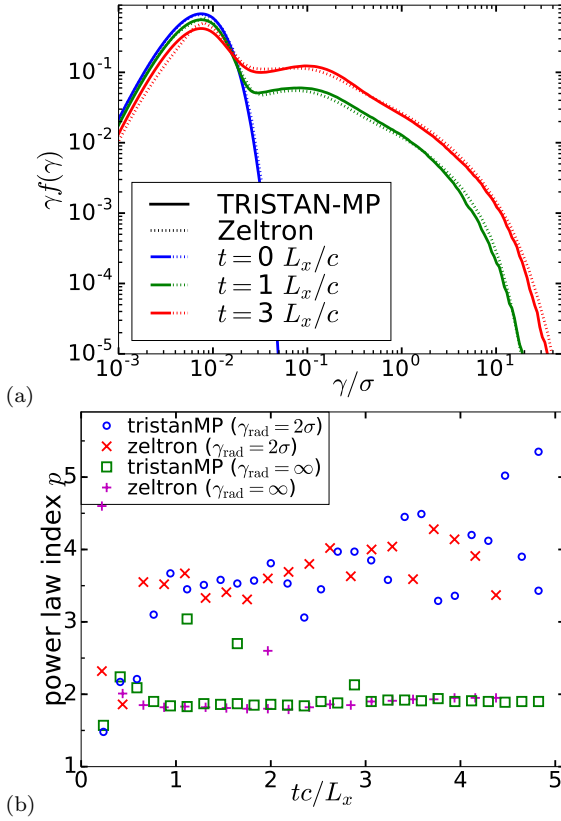


Figure 5. TRISTAN-MP and ZELTRON yield very similar results. (a) Particle energy spectra of TRISTAN-MP (solid lines) and ZELTRON (dotted) at different times for a nonradiative simulation (stochastic fluctuations prevent sufficiently precise comparison of radiative simulations); (b) power-law slopes for $\gamma_{\text{rad}} = 2\sigma$ and ∞ .

(e.g., Kagan et al. 2016) yield broadly similar qualitative features, such as spectral steepening, a useful quantitative comparison will require a future synchrotron study that systematically varies radiation strength as in this study.

The robust dichotomy of nonthermal spectra produced by reconnection with IC cooling has important implications for understanding radiative kinetic plasma processes in astrophysical systems like BH ADCe. The spectral indices of IC radiation from our simulations of strongly-cooled relativistic reconnection, $\alpha_{\text{IC}} \simeq 1.1$, are close to $\alpha \simeq 1.5$ observed in hard X-ray spectra (believed to come from IC scattering of soft disc photons by energetic coronal electrons) in HS and Steep Power Law XRB states, while $\alpha_{\text{IC}} \simeq 0.5$ seen in weak-cooling simulations is similar to $\alpha \simeq 0.7$ observed in the low-hard states (Remillard & McClintock 2006). In future work we will investigate whether our conclusions about NTPA and radiative signatures still hold in the presence of ions and pair production. We will also study effects of the Comptonization (e.g., secondary scatterings) on the escaping radiation. This will allow first-principles prediction of the IC spectrum of flares powered by magnetic reconnection.

ACKNOWLEDGEMENTS

We thank M. Begelman, A. Beloborodov, E. Quataert, K. Parfrey, L. Sironi, A. Spitkovsky, and V. Zhdankin for

fruitful discussions. This work was supported by DOE grant DE-SC0008409, NASA grants NNX17AK57G and NNX16AB28G, NSF grant AST-1411879, and NASA through Einstein Postdoctoral Fellowship grant PF7-180165 awarded to AP by the Chandra X-ray Center, operated by the Smithsonian Astrophysical Observatory for NASA under contract NAS803060. The simulations presented in this paper used computational resources of the NASA/Ames HEC Program and XSEDE/Stampede2 (allocation PHY140041) (Townsend et al. 2014). DAU gratefully acknowledges the hospitality of the Inst. for Advanced Study and support from the Ambrose Monell Foundation.

REFERENCES

- Beloborodov A. M., 2017, *ApJ*, **850**, 141
- Bhattacharjee A., Huang Y.-M., Yang H., Rogers B., 2009, *Phys. Plasmas*, **16**, 112102
- Cerutti B., Werner G. R., Uzdensky D. A., Begelman M. C., 2013, *ApJ*, **770**, 147
- Cerutti B., Philippov A. A., Spitkovsky A., 2016, *MNRAS*, **457**, 2401
- Esirkepov T. Z., 2001, *Comput. Phys. Commun.*, **135**, 144
- Goodman J., Uzdensky D., 2008, *ApJ*, **688**, 555
- Guo F., Li H., Daughton W., Liu Y.-H., 2014, *Phys. Rev. Lett.*, **113**, 155005
- Hoshino M., Lyubarsky Y., 2012, *Space Sci. Rev.*, **173**, 521
- Jaroschek C. H., Hoshino M., 2009, *Phys. Rev. Lett.*, **103**, 075002
- Kagan D., Sironi L., Cerutti B., Giannios D., 2015, *Space Sci. Rev.*, **191**, 545
- Kagan D., Nakar E., Piran T., 2016, *ApJ*, **826**, 221
- Kirk J. G., Skjæraasen O., 2003, *ApJ*, **591**, 366
- Lyubarsky Y. E., 1996, *A&A*, **311**, 172
- Lyubarsky Y. E., 2005, *MNRAS*, **358**, 113
- Lyutikov M., Uzdensky D., 2003, *ApJ*, **589**, 893
- Nalewajko K., Yuan Y., Chruślińska M., 2018, *J. Plasma Phys.*, **84**, 755840301
- Petropoulou M., Sironi L., 2018, arXiv:1808.00966,
- Philippov A. A., Spitkovsky A., 2018, *ApJ*, **855**, 94
- Remillard R. A., McClintock J. E., 2006, *ARA&A*, **44**, 49
- Sironi L., Spitkovsky A., 2014, *ApJ Lett.*, **783**, L21
- Spitkovsky A., 2005, in Bulik T., Rudak B., Madejski G., eds, *AIP Conf. Proc. Vol. 801*, 345
- Tamburini M., Pegoraro F., Di Piazza A., Keitel C. H., Macchi A., 2010, *New J. Phys.*, **12**, 123005
- Towns J., et al., 2014, *Comput. Sci. Eng.*, **16**, 62
- Umeda T., Omura Y., Tominaga T., Matsumoto H., 2003, *Comput. Phys. Commun.*, **156**, 73
- Uzdensky D. A., 2016, in Gonzalez W., Parker E., eds, *Astrophysics and Space Science Library Vol. 427, Magnetic Reconnection: Concepts and Applications*. Springer-Verlag, p. 473
- Uzdensky D. A., Spitkovsky A., 2014, *ApJ*, **780**, 3
- Uzdensky D. A., Loureiro N. F., Schekochihin A. A., 2010, *Phys. Rev. Lett.*, **105**, 235002
- Uzdensky D. A., Cerutti B., Begelman M. C., 2011, *ApJ Lett.*, **737**, L40
- Werner G. R., Uzdensky D. A., 2017, *ApJ Lett.*, **843**, L27
- Werner G. R., Uzdensky D. A., Cerutti B., Nalewajko K., Begelman M. C., 2016, *ApJ Lett.*, **816**, L8
- Yuan Y., Nalewajko K., Zrake J., East W. E., Blandford R. D., 2016, *ApJ*, **828**, 92
- Zweibel E. G., Yamada M., 2009, *ARA&A*, **47**, 291

This paper has been typeset from a $\text{\TeX}/\text{\LaTeX}$ file prepared by the author.